Stress-Radiation–Induced Swelling in Plastic Capsules

Introduction

Unique and distinctive features on the inner surface of plastic capsules used in deuterium–tritium (DT) inertial confinement fusion (ICF) experiments on OMEGA[1] were observed when the capsules were permeation filled to provide cryogenic ignition-scale targets. The features were not observed when deuterium (D_2) was substituted for DT nor were they observed in similar targets filled at the National Ignition Facility (NIF) with DT through a narrow fill tube (<10-μm inner diameter) (Ref. 2). The size and number of these features did not change when the capsules were warmed above 40 K. A capsule warmed to 300 K without rupturing was recovered and inspected using electron microscopy. The features were smaller than 100 nm high and are not expected to impair the hydrodynamic stability during the implosion.[3] Despite their small size, the features are sufficiently noticeable that their origin and magnitude should be understood and eliminated if possible.

The likely cause of these features was deduced through a process of elimination: the features were not present before the capsules were filled with DT and appeared once the targets were cold (19 K) and filled with DT. These features did not grow in size or number after they were first observed; they possessed a sizeable footprint (>20-μm diameter) and were less than 100 nm high. No pore structure or voids (>20 nm, the detection limit) were observed in or below the features, and no blisters were formed by subsurface pressurized voids. The best explanation for their origin is that they arise from the radiation dose imparted to the plastic, combined with the stresses experienced by the capsules during gas permeation and/or transfer of the capsule at cryogenic temperatures (25 to 40 K). While it is well known that β-radiation ruptures carbon–carbon and carbon–hydrogen bonds to generate volatile species,[4] it is postulated that at very high doses and while under stress, the high density of $C_xH_y^*$ radicals and dissolved deuterium–tritium gas present in the polymer structure may recombine to form a material with a lower density in localized areas. This would cause volumetric swelling, and buckling would be more likely to occur at the inner surface because that region receives the highest dose. This would be a soft-matter analogue to stress–corrosion behavior in metals where a combination of stress and a corrosive environment accelerates chemical changes. This article describes the observed features, the radiation doses, and stress levels that the capsule experiences when it is processed to produce a cryogenic DT target.

Observed Defects

All the targets discussed here were provided by General Atomics and processed through the OMEGA Cryogenic Target Handling System using permeation-filling, cooling, and transporting protocols that are well established.[5] Figure 132.8(a) shows a DT-filled target (0.86-mm outer diameter; 10-μm plastic wall; 95-μm ice layer) at 19.5 K with several distinctive features, two of which are the topic of this article. These features were subsequently identified to be on the inner surface of the plastic wall. Figure 132.8(b) shows that same target at 227 K with the features in the same location possessing the same shape, indicating that the features were not condensed gas that had formed on the capsule. Features with similar shapes and in similar numbers (1 to 5) were observed in most but not all of the DT-filled targets.

Attempts to recover DT-filled cryogenic targets from the cryostat had limited success; all the targets except one exploded as the target warmed and the DT evaporated. In this instance the rate of temperature (and therefore pressure) rise was slower than the rate at which gas permeated out of the capsule so that the burst pressure was not exceeded. The capsule was examined optically and then fractured to image the inner surface with electron microscopy.

Figure 132.9 shows electron microscopy images of the features on the inner surface. Two separate features were imaged using backscattered-electron [Figs. 132.9(a) and 132.9(c)] and secondary-electron [Figs. 132.9(b) and 132.9(d)] modes of operation. The backscattered signal arises from incident electrons elastically scattered off atoms at the surface and is more sensitive to the elemental composition of the surface than is the signal obtained from secondary electrons. Images from the backscattered signal show greater contrast between the
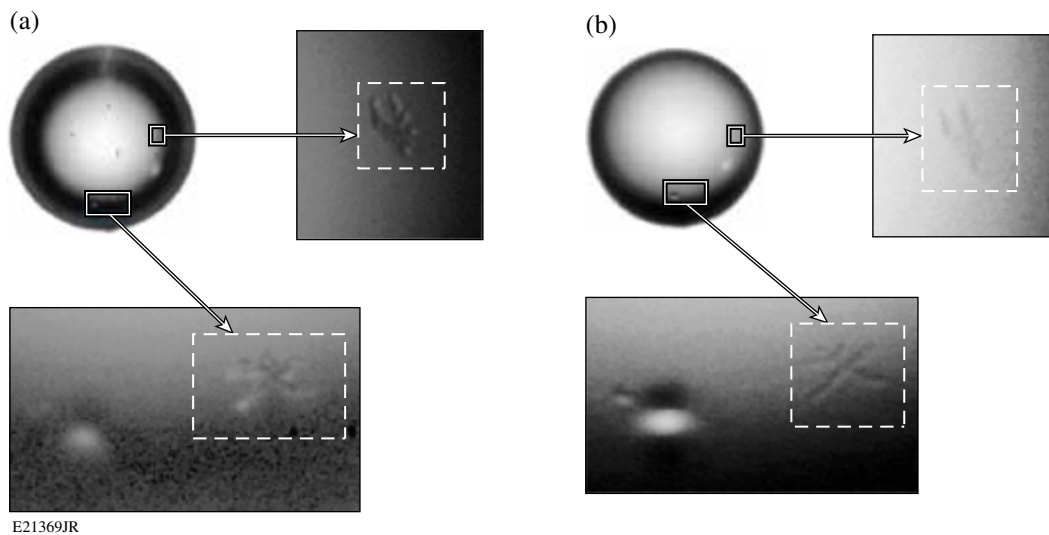
Figure 132.8
A DT-filled target is shown with two distinctive features at (a) 19.5 K and (b) 227 K. Both images were acquired while the target was inside the moving cryostat and were imaged using the existing shadowgraphy optical system. The insets show the features magnified digitally.

features and the plastic shell than could be obtained from the secondary-electron signal, suggesting that the feature could be associated with a difference in the elemental composition of the material; for example, a difference in the ratio of carbon to hydrogen atoms.

Viewing these features at an oblique angle (Fig. 132.10) provided topographic information: the two-dimensional (2-D) pattern seen in Figs. 132.8 and 132.9 is seen as a series of small domes less than 0.1 μm high when the surface is imaged from an angle of less than 50° to the surface. Imaging the edge of the shell wall at the location where the fracture intersects the dome features revealed no deep-level porosity or void structure [Figs. 132.10(a) and 132.10(b)]. No porosity was observed beneath the dome when a 0.5- $\times$ 0.5-μm-sq–shaped, 0.2-μm-deep depression was etched into the dome by repeatedly rastering the electron beam across the surface [Fig. 132.10(b)].
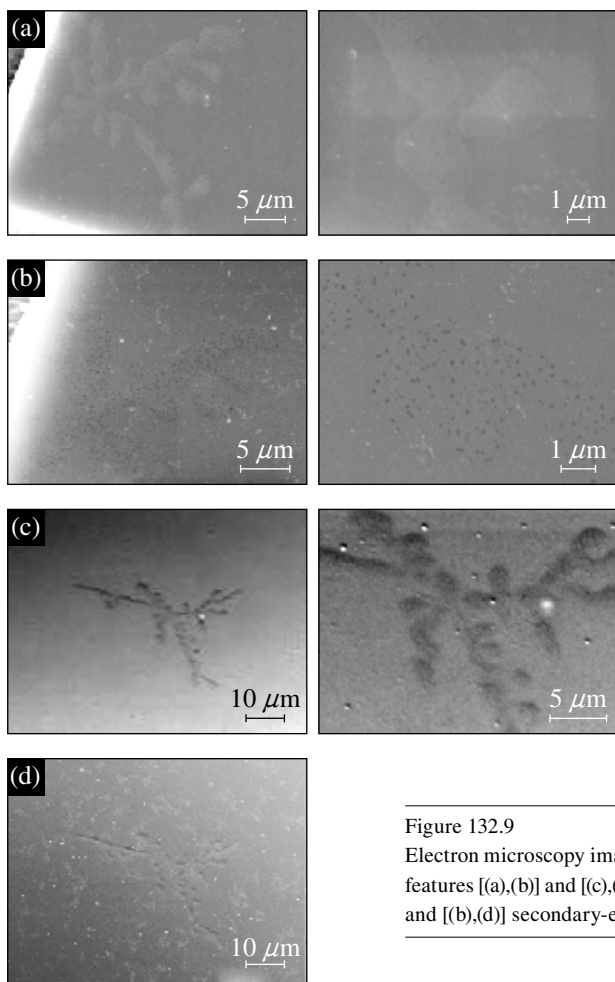
Figure 132.9
Electron microscopy images of the inner surface of the plastic shell recovered from the moving cryostat. Two features [(a),(b)] and [(c),(d)] were imaged and each image was acquired in both [(a),(c)] backscatter signal mode and [(b),(d)] secondary-electron mode. The insets show the features at higher magnifications.
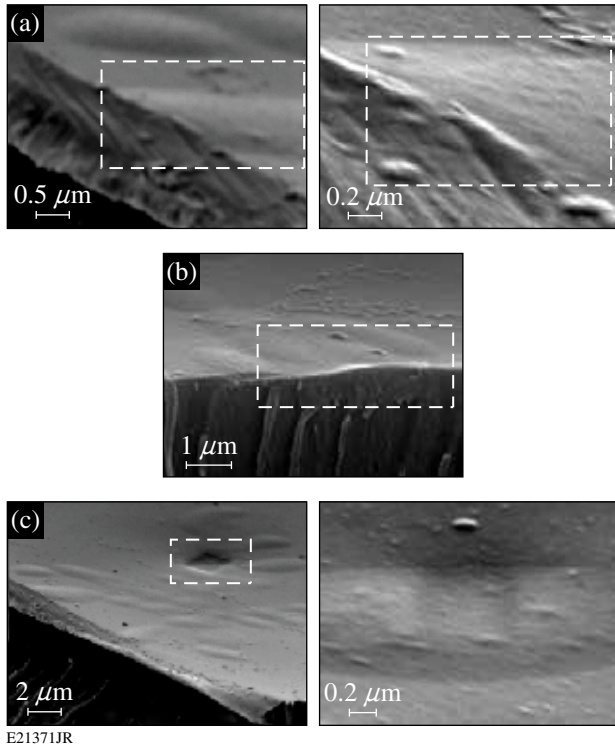
E21371JR

Figure 132.10
The secondary-electron images of the features taken at oblique angles. [(a),(b)] Images are of cross sections through the plastic wall and two domed features (highlighted in the box). The areas highlighted by the rectangular boxes are the regions where the domes intersect the fractured edge of the plastic capsule. (c) A square indentation (denoted by the rectangular box) was etched into the plastic and imaged to see if subsurface porosity was present (it was not).

Radiation Dose and Damage to the Plastic Capsule

Tritium has a half-life of 12.3 years and decays into ^{3}He, releasing an electron with a mean energy of 5.7 keV and a maximum energy of 18.6 keV (Ref. 6). The electron loses energy due to ionization and excitation as it propagates through a medium according to Bethe's relationship:[7]

$$dE/dx = 2\pi e^4 nZ\left[\ln\left(E/I\right)/E\right],$$

where E is the kinetic energy of the electron at position x, n is the number density, Z is the atomic number, and I is the average ionization and excitation energy of the absorber. The effect is that the electron flux to the plastic wall is, to the first order, independent of the DT-gas pressure: electron generation and self-absorption are equally proportional to the tritium density, so increasing the tritium density decreases the shell thickness of tritium near the capsule wall that generates the electron flux that strikes the plastic. The penetration range of the mean and the maximum electron energies in DT and plastic are shown in Table 132.II.

Calculating the dose to the plastic wall assumes that the attenuation of the electron energy is linear with distance. The electron flux (ϕ) to a surface is

$$\phi = \left(1/6\right)\int_0^R \left(1 - x/R\right)\lambda n \, dx,$$

where x is the distance traveled normal to the plastic surface, R is the range of the electron, n is the tritium number density, λ is the probability of tritium atom decay, and the dose (D) is

$$D = E\phi/\rho_m R_m = En\left[\lambda/\left(\rho_m R_m\right)\right]R_T/4,$$

where m is the mass of the absorbing region, ρ_m is the density of the region, R_m is the range in the absorbing region, and R_T is the average range of a 5.7-keV electron in the tritium gas.[8]

The plastic capsules experienced a dose of 259 Mrad during the 17.3 h required to permeation fill the target to 700 bar and the 16.3 h to cool the target to 26 K [Fig. 132.11(a)]. The plastic experienced an additional dose of 136 Mrad during the subsequent 34 h required to form and characterize the ice layer [Fig. 132.11(b)]. Increasing the time to fill the capsule to provide a thicker ice layer, or to permeate through a thinner plastic wall increased the dose to the plastic proportionally. A

Table 132.II: Electron ranges in relevant material.

Material	Density (g/cm^3)	Range for 5.7-keV electrons (μm)	Range for 18.6-keV electrons (μm)
DT (1 bar)	0.000223	2786	35571
DT (10 bar)	0.00223	280	3557
DT (50 bar)	0.0115	57	711
DT (700 bar)	0.156	4	50
DT (ice at 19.7 K)	0.25	2.3	29
Plastic	1.06	0.4	5

(a)   Gas filling and cooling ~30 h
        (34% DT)

(b)   Layer formation and maintenance
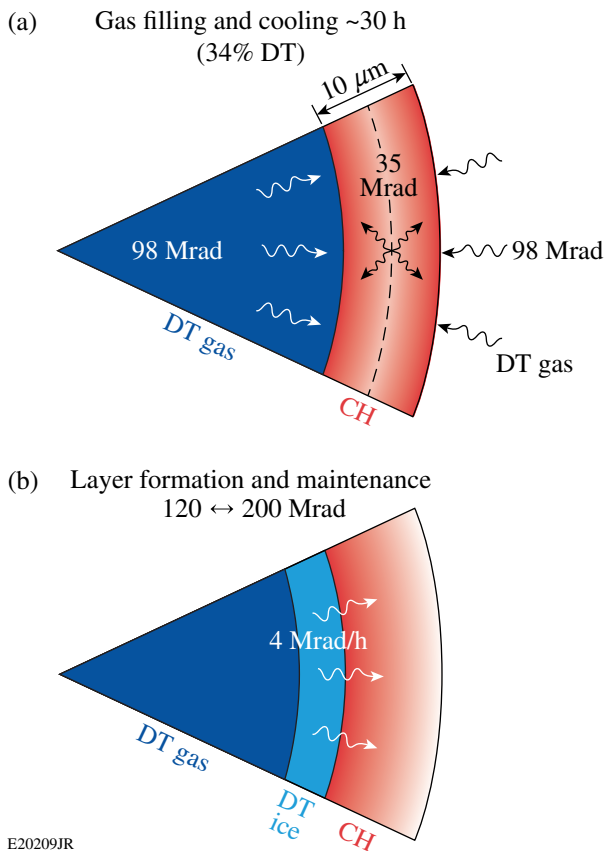   120 ↔ 200 Mrad

Figure 132.11
A schematic showing the electron dose to the plastic surface from (a) the gas inside and outside the capsule and the gas dissolved in the plastic during the permeation and cooling phase, and (b) the gas/liquid/ice inside the capsule during the layer formation and target storage period before the target is imploded.

portion of this dose was delivered to the plastic from the tritium dissolved in the plastic wall. This dose was

$$D = n(1/\rho)\lambda E,$$

where n is the concentration of tritium atoms in the material, ρ is the material density, and E is the mean β energy that varied during the pressure ramp as the amount of DT dissolved in the plastic is ~10% of the surrounding gas density. The solubility of deuterium in the plastic was not known; however, it may be estimated from the known solubility of hydrogen in polymers with comparable densities and elemental composition: neoprene has a solubility of 0.014 scc/cc-atm, corresponding to a dose of 35 Mrad for the 30-h–duration filling and cooling process.

Features attributed to tritium damage were present when the target was first observed after filling. No additional features

developed while the ice layer was formed and until the target was imploded (up to 3 weeks). This suggests that a radiation dose alone is not a sufficient condition for the formation of features, but the absence of these features in D_2-filled shells indicates that it is a necessary condition.

These calculations are a conservative estimate since they assume an average electron energy of 5.7 keV, whereas the actual energy distribution is non-Gaussian and is skewed to higher energy values.

Stresses that Develop During Permeation Filling and Cryogenic Transport
The process of filling targets by permeation, cooling them, and transporting them from the permeation cell to individual moving cryostats subjects the capsules to compressive and tensile stress that approaches the limits for the plastic material (~60 MPa).

DT is permeated into the capsule at 295 K over a 24-h duration and subjects the capsules to a constant compressive stress. The magnitude of the compressive stress is limited by the buckling pressure of the shell, which is ~0.3 to 1 MPa for capsules with the dimensions used here (wall thickness was 5 or 10 μm) (Ref. 9). These stress levels are a worst-case instantaneous load averaged over the entire shell wall and the time-averaged compressive stress is ~0.2 MPa. Compressive stresses greater than 1 MPa could arise from near-instantaneous pressure spikes that occur as a result of isolated events (such as compressibility changes in the hydraulic fluid or rapid volume changes associated with valves closing) over a time interval that is shorter than the measurement duration of the pressure sensor (~2 s). Further, regions of the plastic wall that deviate from perfect circularity could experience approachably higher localized stress as the compressive hoop stress becomes increasingly a shear stress depending on the deviation from circularity.

Cooling the target from 300 K to 26 K (to recover the gas inside the pressure vessel but outside the capsule) takes 18 h and subjects the capsule to a maximum burst pressure of 0.8 bar (Ref. 10), equivalent to a tensile stress of 0.081 MPa (Fig. 132.12). As the target approaches 26 K, a compressive load forms (~0.1 MPa) on the capsule wall. This buckle pressure is an unavoidable consequence of the construction of the equipment that requires the pressure vessel to be sealed with a valve at 300 K (to avoid leakage), and the lower density of the warm gas near the valve results in a higher gas pressure outside the capsule than inside it. Removing the DT gas surrounding the capsule removes the compressive stress in the
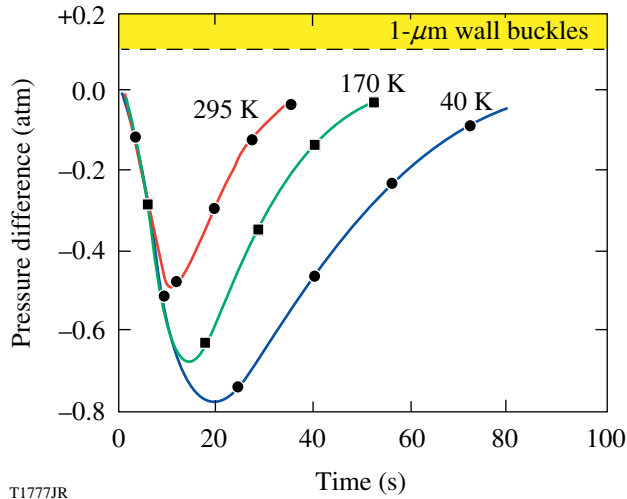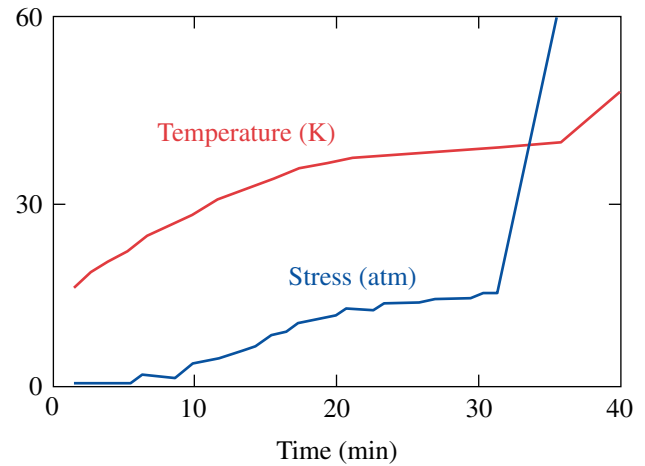
Figure 132.12
Time-dependent average burst pressure exerted on the plastic capsule wall when it was cooled by 1 K. The three curves show the effort of the 1-K temperature step at three separate temperatures: 295 K, 170 K, and 40 K.

overheated and ruptured during a transfer process that took too long to complete; a portion of the plastic shell is missing and features in the plastic wall appear similar to those imaged with the electron microscope.
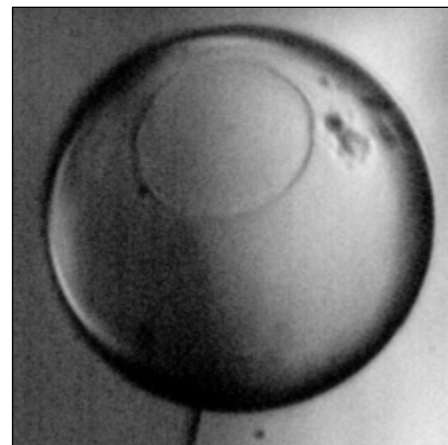
One experiment that demonstrated the importance of stress on the formation of the features was to include a capsule with a

Figure 132.13
Calculated rise in temperature and pressure of a DT target when it was transferred from the permeation cell to the moving cryostat inside the Fill/Transfer Cryostat. β decay is the sole heat source.

plastic and replaces it with a 0.16-MPa tensile stress, resulting from the vapor pressure of liquid DT inside the capsule. A prolonged cyclic stress in the plastic that varies between compressive and tensile is a consequence of these permeation and cooling operations.

Once the capsule has the desired DT inventory, there is a constant heat source inside the capsule from β decay (up to 9 μW) and a heat-exchange gas cools the target. The pressure of the gas must be greater than 100 Pa for cooling to be most effective. The temperature of the capsule (and therefore the pressure in the capsule) depends on the temperature of the boundary (the permeation cell or cryostat) and the distance between the capsule and the boundary. Capsules are maintained below 19 K inside the permeation cell and at an external pressure of 250 Pa (helium). Transferring capsules to the moving cryostat is the process that induces the greatest known stress in the capsule wall, which approaches, and in some cases exceeds, the ultimate yield strength of the plastic. This occurs because the cooling process is inefficient [the helium cooling gas pressure in the cryostat is low (7 Pa), and the distance between the capsule and the cold surface is large (>15 cm)] and the process is lengthy. The capsule begins the transfer process at ~16 K and has taken up to 45 min to be inserted into the moving cryostat and cooled back to 19 K. The calculated rate of increase in the pressure inside the capsule during this process is shown in Fig. 132.13. This calculation includes the temperature-dependent heat capacity, heat-of-fusion, and heat-of-evaporation of DT. Figure 132.14 shows a target that

Figure 132.14
Image of a ruptured target inside the moving cryostat that overheated during transfer. A circular portion of the capsule is missing. Note the presence of a sizeable feature near the rupture area that is similar to the features identified as domes in the target (Fig. 132.8) that was recovered.

hole in it with other intact capsules in a fill cycle. This subjected all the capsules to the same radiation dose but the capsule with the hole did not experience the stresses experienced by the other capsules during the permeation, cooling, and transport phases. No evidence of these features was observed in the capsule containing the hole.

Improvements in the equipment and process used to transfer targets to the moving cryostat decreased the time required for the transfer and allowed for a higher helium gas pressure to be used in the moving cryostat. This substantially reduced the number of defects in the capsules.

Radiation-Relevant Properties and Behavior of ICF Capsules

Plastic capsules for ICF experiments are made using a vapor-phase, glow-discharge polymerization process where hydrocarbon radicals are formed in a low-temperature plasma and deposited on a mandrel that is subsequently removed.[11] The carbon-to-deuterium atomic-percent ratio is 0.53:0.47. The fraction and distribution of carbon–hydrogen and carbon–carbon single, double, and triple bonds throughout the capsule wall are stochastic. The polymer cannot be characterized by a molecular weight and the material is better defined as an amorphous hydrocarbon structure where on average one carbon atom is bonded to at least two other carbon atoms to form the structural backbone, and one carbon is bonded to two or three deuterium atoms to form branching side chains. No information regarding the radiation toughness of this material is available, although the material may be expected to have slightly higher radiation toughness than materials with comparable elemental ratios (such as polystyrene) because of the higher carbon-to-deuterium ratio and greater fraction of carbon–carbon double and triple bonds. It is speculated that the regions of the plastic wall that exhibit the domed features possess a locally higher fraction of species that are more likely to experience a density change when the chemical bonds are broken and subsequently rearranged.

Radiation damage from β electrons will rupture carbon–carbon and carbon–deuterium bonds (bond energies are 3.3 eV/bond and 3.9 eV/bond, respectively) at a high rate given the 5.7-keV mean energy of the electrons and flux of 7.4×10^9 electrons/s, which equates to 10^{13} bond ruptures per second. The majority of the bonds subsequently reform; however, carbon atoms may reform with neighboring carbon atoms rather than the ones from which they separated (possibly making double or triple bonds), or they may bond with nearby deuterium

atoms formed in the D–T $\rightarrow$ D + ^{3}He + e$^-$ (5.7-keV) dissociation process. Should sufficient changes occur in a localized region of the capsule wall, the density and mechanical properties of the area will be altered. The behavior of an alternative plastic material with an estimated lower radiation toughness [poly(α-methyl)styrene (PAMS)] based on its structure was tested by filling a comparably dimensioned PAMS capsule with DT. (Capsules made from PAMS and glow-discharge polymerizations are the only ones available for testing and neither material has known radiation toughness values.) A feature larger than those typically observed in standard GDP (glow-discharge plasma) shells was observed in the PAMS capsule (Fig. 132.15).
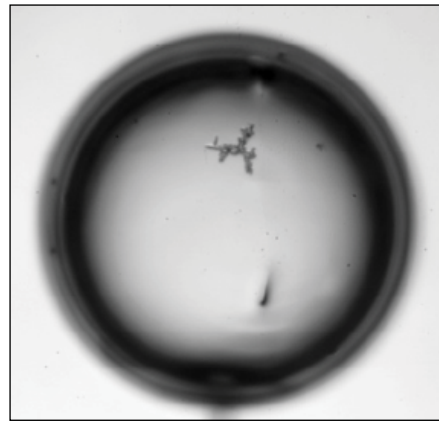
E21373JR

Figure 132.15
Image of a feature in a PAMS [poly(α-methyl)styrene] shell that was filled with DT along with standard GDP (glow-discharge plasma) shells.

Conclusion

Domed-shaped defects with large footprints (>20 μm) and small heights (<0.1 μm) were observed on the inside surface of plastic ICF shells that were permeation filled with DT and cooled to form ignition-scale targets. These features were not present on targets that were processed similarly and filled with D$_2$ instead of DT nor were they present on targets filled through a fill tube. A combination of high-radiation doses and stress levels inside the plastic wall were required for their formation. It is unclear which stage of the permeation filling, cooling, and transfer steps was responsible for their formation; however, it is clear that these features do not propagate in size or number once the ice layer has formed. There was no evidence of any porosity in these features nor were these features a result of blistering. These observations, combined with data from backscatter- and secondary-electron microscopy, suggest that the scission and reformation of carbon–carbon and carbon–hydrogen bonds may cause a localized decrease in the density of the material

that is manifested as a small-scale swelling. Other possible causes are not precluded, although no other mechanism has been identified that is consistent with all the data.

REFERENCES

1. V. N. Goncharov, T. C. Sangster, T. R. Boehly, S. X. Hu, I. V. Igumenshchev, F. J. Marshall, R. L. McCrory, D. D. Meyerhofer, P. B. Radha, W. Seka, S. Skupsky, C. Stoeckl, D. T. Casey, J. A. Frenje, and R. D. Petrasso, Phys. Rev. Lett. **104**, 165001 (2010).

2. E. Mapoles, Lawrence Livermore National Laboratory, private communication (2011).

3. T. J. B. Collins, J. A. Marozas, K. S. Anderson, R. Betti, R. S. Craxton, J. A. Delettrez, V. N. Goncharov, D. R. Harding, F. J. Marshall, R. L. McCrory, D. D. Meyerhofer, P. W. McKenty, P. B. Radha, A. Shvydky, S. Skupsky, and J. D. Zuegel, Phys. Plasmas **19**, 056308 (2012).

4. E. A. Evans, *Tritium and Its Compounds*, 2nd ed. (Wiley, New York, 1974).

5. D. R. Harding, T. C. Sangster, D. D. Meyerhofer, P. W. McKenty, L. D. Lund, L. Elasky, M. D. Wittman, W. Seka, S. J. Loucks, R. Janezic, T. H. Hinterman, D. H. Edgell, D. Jacobs-Perkins, and R. Q. Gram, Fusion Sci. Technol. **48**, 1299 (2005).

6. K. C. Jordan, B. C. Blanke, and W. A. Dudley, J. Inorg. Nucl. Chem. **29**, 2129 (1967).

7. G. F. Knoll, *Radiation Detection and Measurement*, 3rd ed. (Wiley, New York, 2000).

8. Canadian Fusion Fuels Technology Project, Ontario, Canada, CFFTP Report I-9219 (1992).

9. A. Nikroo *et al.*, Fusion Sci. Technol. **45**, 229 (2004).

10. E. L. Alfonso, R. Q. Gram, and D. R. Harding, Fusion Sci. Technol. **45**, 218 (2004).

11. S. A. Letts *et al.*, Fusion Technol. **28**, 1797 (1995).